Remote Sensing of Environment 115 (2011) 3507–3516

Contents lists available at SciVerse ScienceDirect

Remote Sensing of Environment

journal homepage: www.elsevier.com/locate/rse

Topographically based spatially averaging of SAR data improves performance of soil moisture models

T.S. Gala [a], D.A. Aldred [b], S. Carlyle [a], I.F. Creed [a,b,*]

[a] Department of Geography, University of Western Ontario, London, Ontario, Canada N6A 5B7
[b] Department of Biology, University of Western Ontario, London, Ontario, Canada N6A 5B7

ARTICLE INFO

Article history:
Received 9 October 2010
Received in revised form 19 August 2011
Accepted 21 August 2011
Available online 14 September 2011

Keywords:
Remote sensing
Topography
Soil moisture
Synthetic aperture radar
RADARSAT-1
LiDAR
Prairie pothole
Canada

ABSTRACT

Spatial averaging schemes have often been used to improve empirical models that relate radar backscatter coefficient to soil moisture. However, reducing the noise in backscatter response not related to soil moisture often results in signal losses that are related to soil moisture. In this study we tested whether a spatial averaging scheme based on topographic features improved regressions relating backscatter coefficient and soil moisture on the low relief landscape of the Prairie Pothole Region of Canada. Soil moisture data were collected along hillslope transects within pothole drainage basins at intervals coincident with RADARSAT-1 satellite overpass. Spatial averaging schemes were designed at four scales: pixel, topographic feature (uplands, sideslopes, and lowlands), pothole drainage basin, and landscape (0.8 km × 1.6 km). The relationship between soil moisture and backscatter coefficient improved with increasing area of spatial averaging from a pixel ($R^2 = 0.18$, $P < 0.005$), to the pothole drainage basin ($R^2 = 0.36$, $P < 0.005$), to the landscape ($R^2 = 0.66$, $P < 0.005$). However, the strongest relationship ($R^2 = 0.72$, $P < 0.005$) was obtained by spatially averaging radar images based on topographic features. These findings indicate that topographically based spatial averaging of RADARSAT-1 imagery improves empirical models that are created to map the complex patterns of soil moisture in prairie pothole landscapes.

1. Introduction

Satellite-based radar data holds great promise for mapping soil moisture over large or inaccessible areas because of the sensitivity of microwave energy to soil moisture content and the ability of microwaves to penetrate clouds and low-density vegetation. However, microwaves also interact with other surface characteristics such as geometry, roughness and vegetation water content to produce a composite signal. In this paper we explore a spatial technique for improving the separation of soil moisture from other surface signals in radar data in the topographically complex landscapes of the Prairie Pothole Region of central North America (Fig. 1).

Models for retrieving soil moisture from radar sources can be classified as complex semi-empirical and simple empirical models. Semi-empirical models include parameters determined from theoretical interactions between surfaces and microwave energy that attempt to account for confounding surface characteristics, but these parameters are difficult to retrieve in the field (e.g., Lievens et al., 2010, 2009; Verhoest et al., 2008). In contrast, empirical models relate the radar backscatter coefficient directly to soil moisture. Spatial averaging is used to improve empirical models by averaging the inherent heterogeneity from random noise or difficult-to-quantify sources associated with backscatter response in a given pixel. Spatial averaging approaches have ranged in size and shape from surrounding pixel neighborhoods (e.g., Moran et al., 2000; Thoma et al., 2008), land patches defined by land use or land cover (e.g., Cognard et al., 1995; Oldak et al., 2003; Quesney et al., 2000), or drainage basins (Álvarez-Mozos et al., 2005). In general, increasing the scale of spatial averaging produces stronger correlations between soil moisture and backscatter coefficient because the inherent heterogeneity of response at the pixel scale is reduced. However, the range and distribution of soil moisture are simultaneously diminished.

It is important to consider the tradeoffs between reducing random backscatter or mixed surface signals and extracting the true soil moisture signal when selecting a spatial averaging scheme. Physical processes controlling soil moisture distribution should be considered in the selection of a spatial averaging scheme. Topography has long been identified as an important control on hillslope geomorphological, hydrological and biogeochemical processes (e.g., Beven & Kirkby, 1979). Topographic features along hillslopes from the uplands through side slopes to lowlands reflect gravitational controls on water and mass movement and have been used to predict soil moisture in a broad range of landscapes (e.g., Famiglietti et al., 1998; Western et al., 1999; Western & Blöschl, 1999). In this paper we explore whether spatial averaging schemes based on topographic features that can

* Corresponding author at: Department of Biology, University of Western Ontario, London, Ontario, Canada N6A 5B7. Tel.: +1 519 661 4265; fax: +1 519 661 3935.
E-mail address: icreed@uwo.ca (I.F. Creed).

0034-4257/$ – see front matter © 2011 Elsevier Inc. All rights reserved.
doi:10.1016/j.rse.2011.08.013

Fig. 1. North American Prairie Pothole Region and Saskatchewan study transect.

be detected from remote sensing sources may better preserve the range and distribution of soil moisture while decreasing the confounding effect of other surface characteristics.

We hypothesize that a process-based approach to defining spatial averaging schemes improves empirical models that relate backscatter coefficient and soil moisture, leading to improved estimation of soil moisture across topographically variable prairie landscapes. We test this hypothesis on a natural (non-agricultural) prairie pothole landscape. The objectives of this study are (a) to develop a spatial averaging scheme based on topographic features identifiable from LiDAR digital elevation data sources; (b) to evaluate the sensitivity of soil moisture expressed in terms of range and distribution to backscatter coefficient in each of the spatial averaging schemes (i.e., pixels, topographic features, pothole drainage basins, and landscape); (c) to compare the strength of empirical models that relate backscatter coefficient to soil moisture for each of the spatial averaging schemes; and (d) to use the strongest model to create maps of soil moisture.

2. Methods

2.1. Experimental design

The Prairie Pothole Region covers about 750,000 km^2 of the Prairie Ecozone of central North America (Fig. 1). Glacial retreat during the Wisconsin period left a landscape with millions of small closed basins commonly called "potholes." Potholes are often underlain by fine glacial till with low permeability that severely limits groundwater discharge and/or recharge, effectively forming ponds fed mainly by surface water from spring snowmelt and rainwater. Potholes range in size, depth and connectivity, but the majority have a surface area <1 ha and rarely become connected through surface hydrologic pathways.

Five 800 m × 1600 m parcels of land were located along a moisture deficit monitoring transect through central Saskatchewan to capture a range of soil moisture conditions from dry in the south (P1) to wet in the north (P5) (Fig. 2). The parcels are covered with grasses of relatively uniform height, density and species composition from June through September (c.f., Fung, 1969; Scott, 1995). These observations allowed for an assumption of homogeneous surface characteristics to be made during this period for the purpose of making direct univariate regressions of soil moisture and backscatter coefficient. An exception to this assumption is the presence of narrow (<3 m) emergent zones surrounding ponds that support the growth of relatively tall grasses, bulrushes and shrubs.

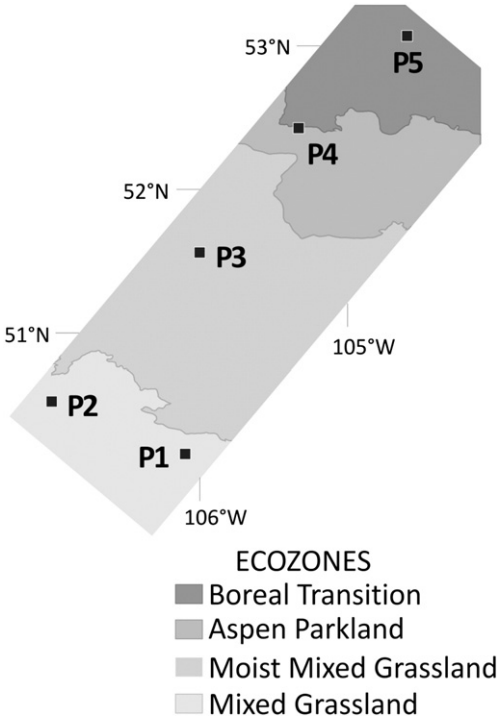

Fig. 2. Study parcels along boreal ecozone transect. Moisture deficits were derived based on 30-year (1975–2005) average annual precipitation (P) recorded at nearby meteorological stations minus potential evapotranspiration (PET) calculated using the method of Hamon (1963): P1 and P2 (P − PET = −520 mm/yr); P3 (P − PET = −420 mm/yr); P4 (P − PET = −300 mm/yr); and P5 (P − PET = −270 mm/yr).

2.2. Volumetric soil moisture content

Soil moisture sampling points were established at 10 m intervals along four cardinal-facing transects from the ridge of the pothole to the point where the soil was inundated or saturated; transects were extended as water drawdown occurred during the summer (Fig. 3). These transects were established in about 20 pothole drainage basins that reflected the distribution of pond permanence classes ranging from ephemeral to permanent in each parcel (Stewart & Kantrud, 1971). Surface soil moisture was measured from June to September 2005 within 24 h of RADARSAT-1 satellite overpasses. Soil impedance (mV) was measured using amplitude time domain reflectometry taken with a ThetaProbe (Delta-T Devices, 1999). Soil impedance readings were taken from the soil surface (0–6 cm); five readings were recorded within a 1 m radius of each sampling point to account for local heterogeneity in soil moisture conditions, and these readings were then averaged to obtain one representative reading per sampling point. Soil impedance readings were converted to volumetric soil moisture content (VSM) using site-specific calibrations (Carlyle, 2006). Geographic coordinates were recorded for each sampling point to allow repeated sampling during subsequent cycles of observation.

VSM data were generalized to the 25 m grid spacing of the corresponding backscatter images. VSM sample points within a 2.5 m buffer of the edges of each 25 m pixel were discarded to reduce the influence of edge values. The remaining VSM sample values were averaged within each 25 m × 25 m grid. The influence of vegetation and surface roughness characteristics at the emergent zone of ponds was eliminated by discarding pixels that intersected surveyed pond boundaries.

2.3. Radar backscatter coefficient

Radar image processing and analytical steps are outlined in Fig. 4. RADARSAT-1 Standard Beam Mode 1 synthetic aperture radar (SAR) images were acquired at 12.5 m pixel spacing in ascending orbit and an approximately 23° incidence angle on June 20, August 7 and

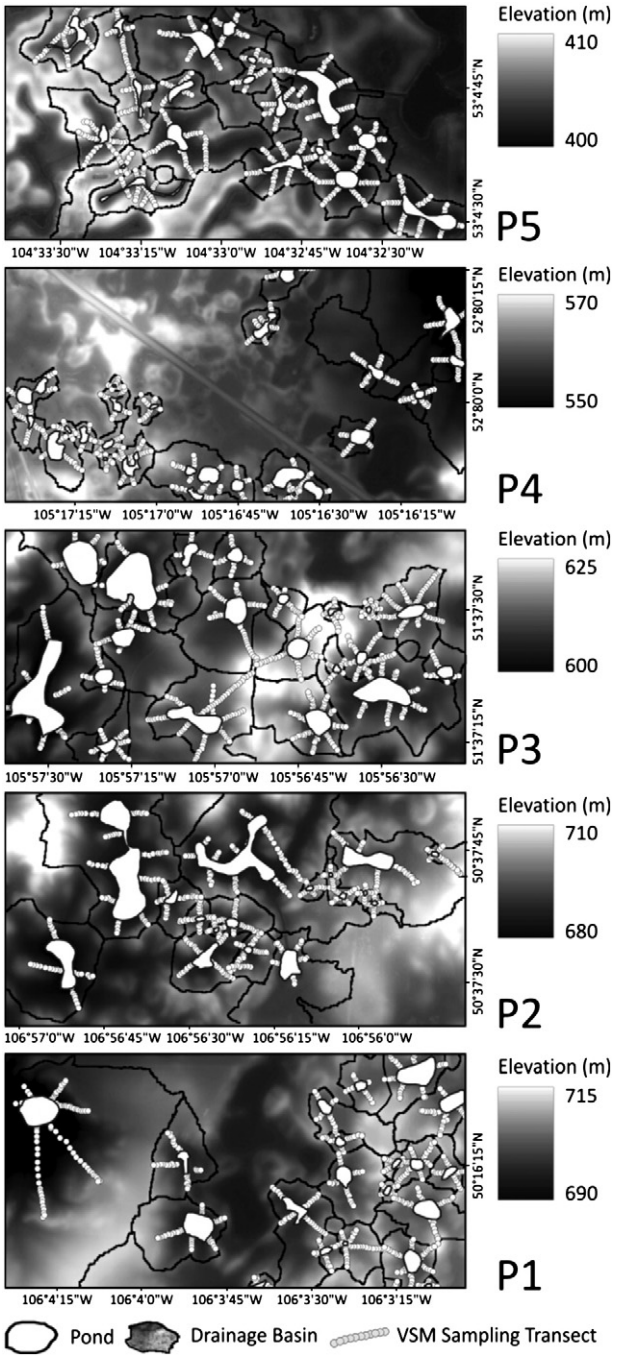

Fig. 3. Locations of VSM sampling ponds and drainage basins showing sampling point transects.

31 at P1 and P2; July 21 and August 14 at P3; July 21 and 28 and August 21 at P4; and July 4 and 28 and August 21 at P5 in 2005. Raw digital numbers were orthorectified, radiometrically corrected for local incidence angles, and converted to unitless backscatter intensity numbers at 25 m pixel spacing. Orthorectification and radiometric corrections were done using a digital elevation model (DEM) resampled from 0.75 arc sec resolution to 18.7 m grid resolution (Government of Canada, 2000) in addition to orbital information and a minimum of eight evenly distributed ground control points collected from hydrographic and road data layers (Government of Canada, 2007a,b). Average root-mean-square errors were <7 m (6.8 m in northing and 6.2 m in easting).

Gamma MAP filters were used to reduce high frequency image noise (i.e., speckle) while maintaining high frequency edges (Lopes et al., 1993). To avoid radiating the effects of specular reflectance in pixels located in inundated ponds onto neighboring pixels, inundated locations were masked out prior to filtering. Pond locations and boundaries were surveyed on the ground at the beginning of the sampling periods using a global positioning system. Because of the ephemeral nature of some of the ponds, inundated locations for each image were estimated by identifying pixels with backscatter intensity ≤ 0.05 (-13 dB) that intersected the surveyed pond locations and applying a 1-pixel buffer. The selected pixels were masked from the image and a Gamma MAP speckle filter using a 3×3 pixel window was applied to the remaining pixels. Radar image processing steps were performed using Geomatica 10.1 (PCI Geomatics, 2007).

2.4. Topographic partitioning of landscapes

DEMs for each parcel were interpolated from LiDAR (Light Detection and Ranging) data (± 0.15 m vertical accuracy) using an inverse distance weighted algorithm to 0.5 m and then resampled to a 2.5 m DEM using a bilinear resampling method. Following MacMillan (2000), a low pass 3×3 mean filter was applied to the DEMs to smooth the effects of elevation noise caused by patterns or trajectories in the original data collection or by relics of interpolation. Filtered 2.5 m DEMs were then rescaled using a linear contrast stretch with no saturation to a fixed range of 0–25 m elevation to provide contrast in slope in parcels with very low relief (e.g., P5).

For each DEM, pothole basin boundaries were determined through a combination of digital terrain analysis and the outer reaches of VSM sampling transects. Topographic features within basins were defined that captured the hydrologic gradient down the hillslopes and that could be resolved at the 25 m pixel spacing of the RADARSAT-1 images. The topographic features included ridges, shoulders (upper convex slopes), side-slopes (concave slopes between uplands and lowlands) and lowlands (relatively flat areas bordering ponds and depressions). These topographic features were mapped using a supervised hierarchical fuzzy classification of topographic attributes.

A classification training data set was generated by collecting samples for identification of topographic features based on heuristics along cross-sectional profiles of the basins. The classification of topographic features was based on the following steps. First, six terrain attributes were derived from the DEMs: (a) percent height relative to local pits and peaks; (b) percent height relative to local channels and divides; (c) topographic wetness index; (d) slope gradient; (e) profile curvature; and (f) plan curvature (see Webster et al., 2011). Second, statistical distributions of the terrain attribute values for each topographic feature were examined to determine the appropriate attributes for separating the features; a terrain attribute was considered to be a useful attribute for separating a given feature when the mean $\pm$ one standard deviation was separated from the means of other features or feature groupings. Third, a fuzzy membership score of a terrain attribute for a topographic feature class was modeled between no membership (0) and full membership (1) in sigmoidal functions. The direction (increasing or decreasing) of the membership function was determined from the relationship of a given feature class mean to other feature class means (e.g., increasing if the given feature class mean was greater than the other feature class means). For an increasing function, the feature class mean value minus one standard deviation was used to define a membership score of 0.5, increasing to full membership at the mean. For a decreasing function, the feature class mean value plus one standard deviation was used to define a membership score of 0.5, decreasing from full membership at the mean. Finally, fuzzy membership scores for each pixel were arithmetically combined and the result converted from a fuzzy to a crisp value to assign a topographic feature or null class for the next rule in the class hierarchy. The rules for the classification, including terrain attributes, membership functions and function transition values for each rule, are outlined in Table 1.

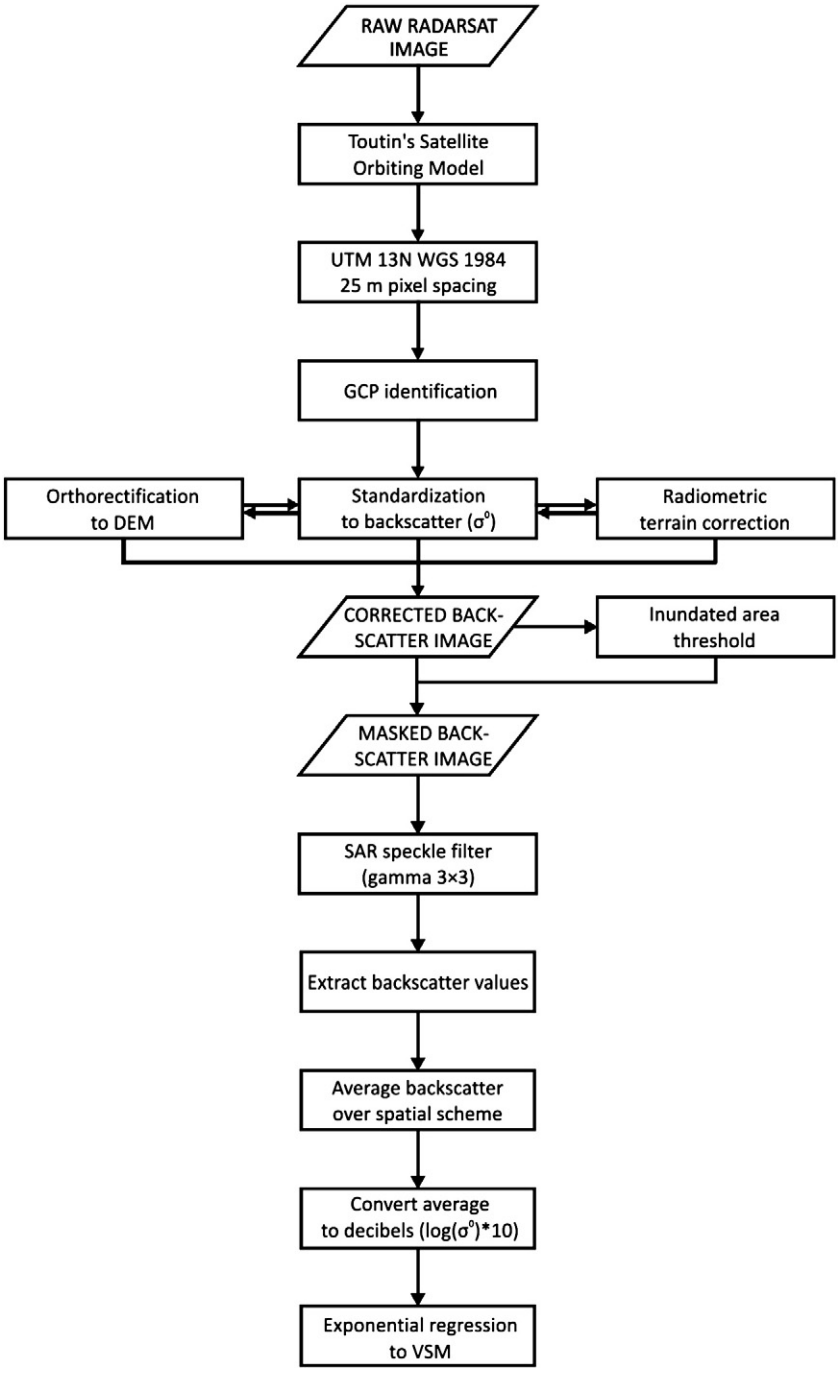

Fig. 4. Flow chart of SAR image processing and analytical steps used in this paper.

The classified topographic features were tested for differences in VSM using a One-Way ANOVA Difference on Ranks test on VSM values at the reference sample points. Median and inner quartile range of VSM were significantly different for the classified topographic features (Fig. 5). Classification maps are shown in Fig. 6. Ground reference data were compared to the classified maps and an overall classification accuracy of 87% was found.

2.5. Spatial averaging schemes

Gridded VSM values were related to backscatter coefficient at four different spatial averaging schemes (i.e., pixel, topographic feature, basin, and parcel). At the pixel scale, backscatter intensity values were converted directly to backscatter coefficient (σ^0) in units of decibels using the formula $\sigma^0 = 10 \times \log_{10}$ (intensity) (Shepherd, 2000). At the topographic feature scale, backscatter intensity and gridded VSM were averaged per topographic feature, per pothole basin, per parcel, and per sampling cycle. At the pothole basin scale, backscatter intensity and gridded VSM values were averaged per pothole basin, per parcel, and per sampling cycle. At the parcel scale, backscatter intensity and gridded VSM values were averaged per parcel and per sampling cycle. At all scales coarser than the pixel, backscatter intensity was first averaged then converted to backscatter coefficient.

2.6. Relating radar backscatter coefficient to volumetric soil moisture

Linear and non-linear regression models relating VSM to backscatter coefficient at each spatial averaging scale were examined for fit.

Table 1
Topographic feature fuzzy classification hierarchy.

Rule	Fuzzy variable	Terrain attribute	Function	Central concept	Dispersion index
1 Ridge	RIDGE1	Slope gradient (%)	Decreasing	2.4	0.9
	RIDGE2	Relative elevation to local channels and divides	Increasing	70	20
	RIDGE3	Plan curvature	Decreasing	−6	6
	If (RIDGE1 × RIDGE2 × RIDGE3) > 0.33, then 'RIDGE', else 'NULL'				
2 Lowland (from rule 1 'NULL' class)	UPPER1	Wetness index	Decreasing	6.2	0.9
	UPPER2	Slope gradient (%)	Increasing	5.3	4
	UPPER3	Relative elevation to local pits and peaks	Increasing	22	16
	LOWER1	Wetness index	Increasing	6.4	1.4
	LOWER2	Slope gradient (%)	Decreasing	7.6	4
	LOWER3	Relative elevation to local pits and peaks	Decreasing	21	12
	If (UPPER1 × UPPER2 × UPPER3) > (LOWER1 × LOWER2 × LOWER3), then 'UPPER', else 'LOWLAND'				
3 Sideslope (from rule 2 'UPPER' class)	SHOULDER1	Profile curvature	Decreasing	0.12	0.3
	If SHOULDER1 > 0.5, then 'SHOULDER', else 'SIDESLOPE'				
4 Upland	'UPLAND' = 'RIDGE' AND 'SHOULDER'				

Simple two-parameter exponential growth regression models ($y = ae^{bx}$) were found to provide similar fits at pixel, basin and parcel scales and an improved fit at the topographic feature scale. As a result, exponential models were developed in addition to linear models at each spatial scale. The relative strengths of the relationships were evaluated using the coefficient of determination (R^2) and the associated P value. The standard error (S.E.) was used to measure the precision of the models. Statistical analyses were performed using SigmaPlot 11.0 (Systat Software, 2008).

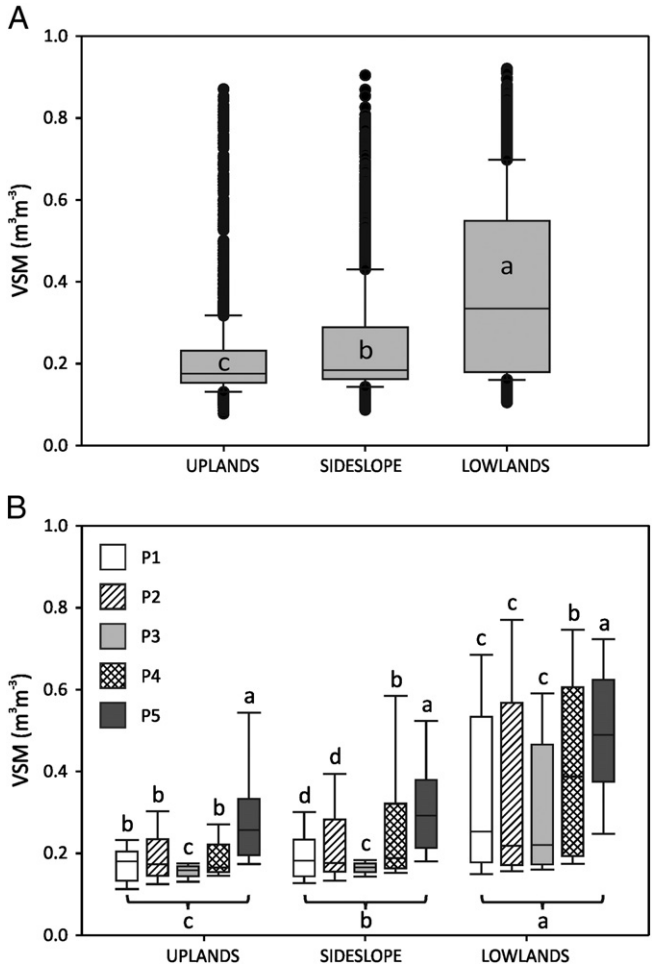

Fig. 5. Box whisker plots of VSM sample values for topographic features (A) and per parcel (B). Boxes show 25th and 75th percentile lines and median in center line, with whiskers marking outliers outside 5th and 95th percentiles. 1997 soil moisture observations were counted in upland features, 2549 observations were counted in sideslope features, and 2407 observations were counted in lowland features. Different letters indicate significant differences in median values as determined by Dunn's pairwise groupings (one-way ANOVA difference on Ranks, $P<0.05$).

At the topographic feature scale, many pixels did not contain uniform topographic features, which limited the number of pixels for the topographic feature scale (n = 104). To examine the effect of sample size from discarding pixels for the topographic feature scale, we randomly selected a number of pixels equal to the number of pixels sampled to develop the topographic feature-averaging scheme (i.e., 104 pixels) and prepared models at the pixel, topographic feature, basin and parcel scales. For the topographic feature scale, the mixed pixels were assigned to a topographic feature using a 50% majority classification. To examine the effect of including only pixels with uniform topographic features, we prepared regression models at the pixel, basin and parcel averaging scales between backscatter coefficient and VSM using only the 104 pixels containing uniform topographic features.

3. Results

3.1. Effects of spatial averaging schemes

The observed backscatter coefficient variation at the pixel scale may be interpreted as random noise, as systematic but unquantified surface effects or as variation in VSM itself. Given a normal distribution of random backscatter noise, a superior spatial averaging scheme will reduce the range in backscatter coefficient due to unwanted or unknown effects but preserve that part of the range that is in response to VSM. Mean backscatter coefficient and VSM did not change significantly between the spatial averaging schemes, while ranges decreased with increasing coarseness of the averaging scales except at the scale of topographic features (Table 2). A 43% reduction in the range of backscatter coefficient from the pixel scale was observed at the topographic features scale (compared to a 29% reduction at the basin scale and a 68% reduction at the parcel scale), while only a 17% reduction in VSM was observed (compared to a 49% reduction at the basin scale and a 73% reduction at the parcel scale). Furthermore, the coefficient of variation (CV) of the backscatter coefficient decreased consistently with increasing spatial average scales, while the CV of VSM was comparable at the spatial average scales of the pixel and topographic feature. In particular, the backscatter coefficient related to VSM in the relatively small lowland areas was preserved with the topographic feature spatial average scheme but lost in the coarser basin and parcel spatial averaging schemes.

The topographic feature spatial average scheme revealed an increase in backscatter coefficient and VSM along the topographic gradient from uplands to lowlands. Mean VSM and backscatter coefficient were both lower in the uplands ($\theta = 0.19\ m^3\ m^{-3}$; $\sigma^0 =$

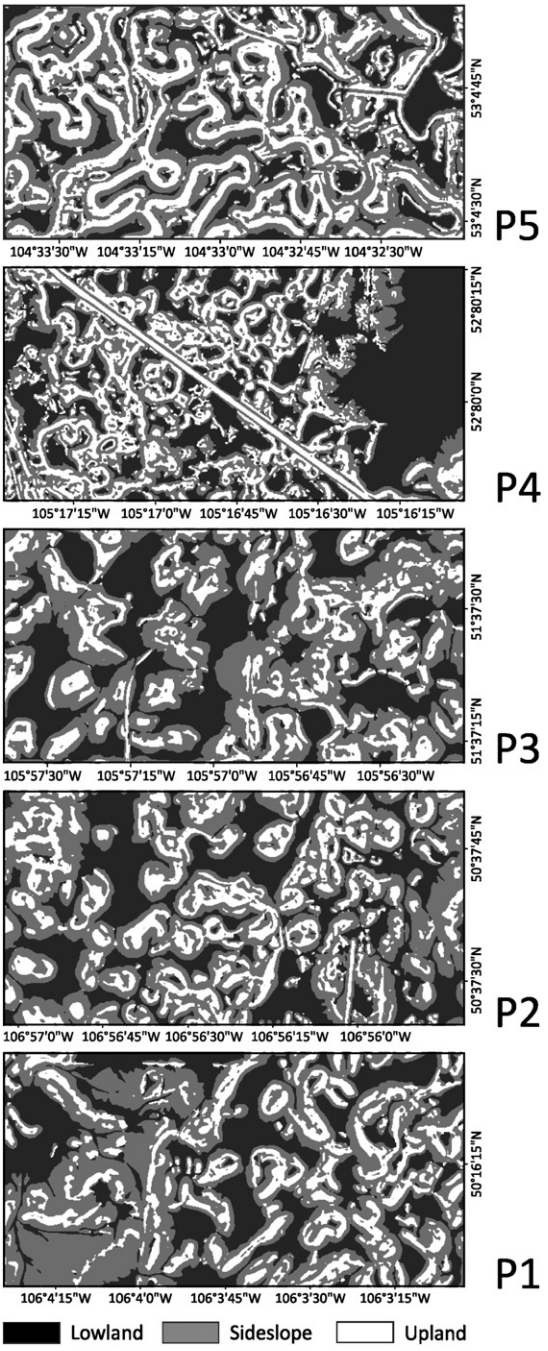

Fig. 6. Topographic feature classification maps.

−5.30 dB) than on the sideslopes ($\theta = 0.22$ m^3 m^{-3}; $\sigma^0 = -4.58$ dB), which were in turn lower than in lowlands ($\theta = 0.28$ m^3 m^{-3}; $\sigma^0 = -4.47$ dB) (Table 3). A one-way analysis of variance on ranks showed a statistically significant difference in median values of both variables between the three topographic features ($P<0.005$).

3.2. Radar backscatter coefficient vs. VSM

Regression models between backscatter coefficient and VSM were fitted by pooling all data at each spatial averaging scale (i.e., from each sampling period and for each parcel). The exponential regression models generally outperformed the linear regression models. While there were no differences or only slight increases in the R^2 of exponential compared to linear models at the pixel, basin and parcel scales, there was a substantial increase at the topographic feature scale (16%) (Table 4).

Table 2
Mean, coefficient of variation and range of volumetric soil moisture (VSM) content (θ) and backscatter coefficient (σ^0) averaged at the pixel, topographic feature, basin and parcel scales.

VSM (θ)	Mean ($m^3\ m^{-3}$)	Standard deviation	Coefficient of variation (%)	Range ($m^3\ m^{-3}$)	Number of observations
Pixel	0.21	0.09	41	0.71	1418
Topographic feature	0.24	0.14	56	0.59	56
Basin	0.21	0.07	33	0.36	218
Parcel	0.21	0.07	31	0.19	14
Backscatter coefficient (σ^0)	(dB)			(dB)	
Pixel	−4.90	1.12	23	8.84	1418
Topographic feature	−4.81	1.01	21	5.02	56
Basin	−4.89	0.97	20	6.24	218
Parcel	−4.83	0.81	17	2.85	14

Among the exponential models, VSM showed a weak relationship with backscatter coefficient at the pixel scale (Fig. 7; Table 4; $R^2 = 0.18$, $P<0.005$). This poor correlation can likely be attributed to (a) positional error, (b) systematic error related to failures in our assumption of homogeneity in surface roughness and vegetation characteristics, and/or (c) random speckle-related noise that remains in the backscatter images even after resampling and filtering. These effects were reduced at coarser spatial averaging scales, leading to improved regressions ($R^2 = 0.36$, $P<0.005$ at the basin scale and $R^2 = 0.66$, $P<0.005$ at the parcel scale). However, the exponential models developed at these scales failed normality and/or constant variance tests.

We found a stronger and statistically significant exponential model at the topographic feature scale (Fig. 7; Table 4; $R^2 = 0.72$, $P<0.005$). Separate regressions fitted to the wetter lowland features and the combined drier sideslope and upland features showed differences in both the slope and strength (R^2) of the exponential models (Fig. 8; Table 5). The exponential model relating backscatter coefficient and VSM for the drier topographic features showed only a slight increase in R^2 (0.20, $P<0.005$) over the model developed at the pixel scale (0.18, $P<0.005$); however, this model passed both normality and constant variance tests. The exponential model for the wetter topographic features showed a substantial increase in R^2 (0.81, $P<0.005$) over the model developed at the pixel scale.

To examine whether the success of the exponential model at the topographic feature scale could be attributed to sampling fewer backscatter image pixels, we randomly selected a number of pixels equal to the number of pixels sampled to develop the topographic feature-averaging scheme (i.e., pixels containing uniform topographic features, n = 104, Table 6). We found that the randomly selected pixel model had similar strength to the original model ($R^2 = 0.18$ vs. 0.17),

Table 3
Mean volumetric soil moisture (VSM) content (θ) and backscatter coefficient (σ^0) averaged at the topographic feature scale per feature type.

VSM (θ)	Mean ($m^3\ m^{-3}$)	Number of observations
Lowland	0.28	31
Sideslope	0.22	19
Upland	0.19	6
Backscatter coefficient (σ^0)	(dB)	
Lowland	−4.47	31
Sideslope	−4.58	19
Upland	−5.30	6

Table 4
Comparison of linear and exponential growth models relating volumetric soil moisture (VSM) to backscatter coefficient averaged at the pixel, topographic feature, basin and parcel scales.

	n	Equation	R^2	S.E.	Normality	Constant variance	P
Linear							
Pixel	1418	$0.37 + 0.03\sigma^0$	0.17	0.08	Failed	Failed	<0.005
Topographic feature	56	$0.71 + 0.10\sigma^0$	0.56	0.09	Failed	Failed	<0.005
Basin	218	$0.41 + 0.04\sigma^0$	0.35	0.06	Failed	Failed	<0.005
Parcel	14	$0.53 + 0.07\sigma^0$	0.66	0.04	Passed	Passed	<0.005
Exponential							
Pixel	1418	$0.46e^{0.16\sigma^0}$	0.18	0.08	Failed	Failed	<0.005
Topographic feature	56	$1.66e^{0.43\sigma^0}$	0.72	0.07	Passed	Passed	<0.005
Basin	218	$0.60e^{0.22\sigma^0}$	0.36	0.05	Failed	Failed	<0.005
Parcel	14	$0.93e^{0.31\sigma^0}$	0.66	0.04	Passed	Failed	<0.005

but the randomly selected topographic feature, basin and parcel scale models were much weaker than the original models ($R^2 = 0.25$ vs. 0.72, 0.18 vs. 0.36, and 0.36 vs. 0.66, respectively). We then examined the effects of including only the same pixel samples used to develop the topographic feature averaging scheme at the pixel, basin and parcel averaging scales. The models improved at each different spatial averaging scheme [$R^2 = 0.56$ vs. 0.18 (pixel); 0.74 vs. 0.36 (basin), 0.80 vs. 0.66 (parcel); Table 7].

The exponential model developed at the topographic feature spatial averaging scale passed both normality and constant variance tests and was applied to a test image comprising an equal distribution of upper and lower topographic features (September 7, P3; this image was not included in the development of the model). Modeled VSM was related to observed VSM data averaged at the topographic feature scale (Fig. 9). There was good agreement between observed and modeled values ($R^2 = 0.81$; $P<0.005$), indicating a useful model.

3.3. Radar mapping of soil moisture in prairie potholes

Maps of VSM using the exponential models developed at the pixel, topographic feature and basin spatial averaging scales were produced (Figs. 10, 11). Topographic features from the 2.5 m classified maps and basins were projected to the 25 m × 25 m grid resolution of the backscatter images using nearest-neighbor resampling before applying the respective model. The maps developed from the topographic feature model captured a large portion of the spatial heterogeneity of VSM in the prairie landscape. The VSM maps captured the increasing trend in soil moisture from uplands to lowlands within pothole basins, and the increasing trend in soil moisture from the drier locations at the southern limit of the moisture deficit gradient (P1) to the wetter locations at the northern limit (P5) (Fig. 10). The VSM maps also captured the temporal trend from the dry summer months (July and August) to wetter fall months (Fig. 11).

4. Discussion

In this paper we explored improvements in the spatial averaging of backscatter coefficient from SAR data for the purpose of extracting surface VSM information from natural prairie pothole landscapes. We determined that topographic features from a classification of terrain attributes derived from LiDAR DEMs are the smallest physically based control on water movement identifiable from remote sensing sources. We compared the effect of spatial averaging at this scale on capturing VSM while reducing backscatter response to random or unquantified surface effects unrelated to VSM with other spatial

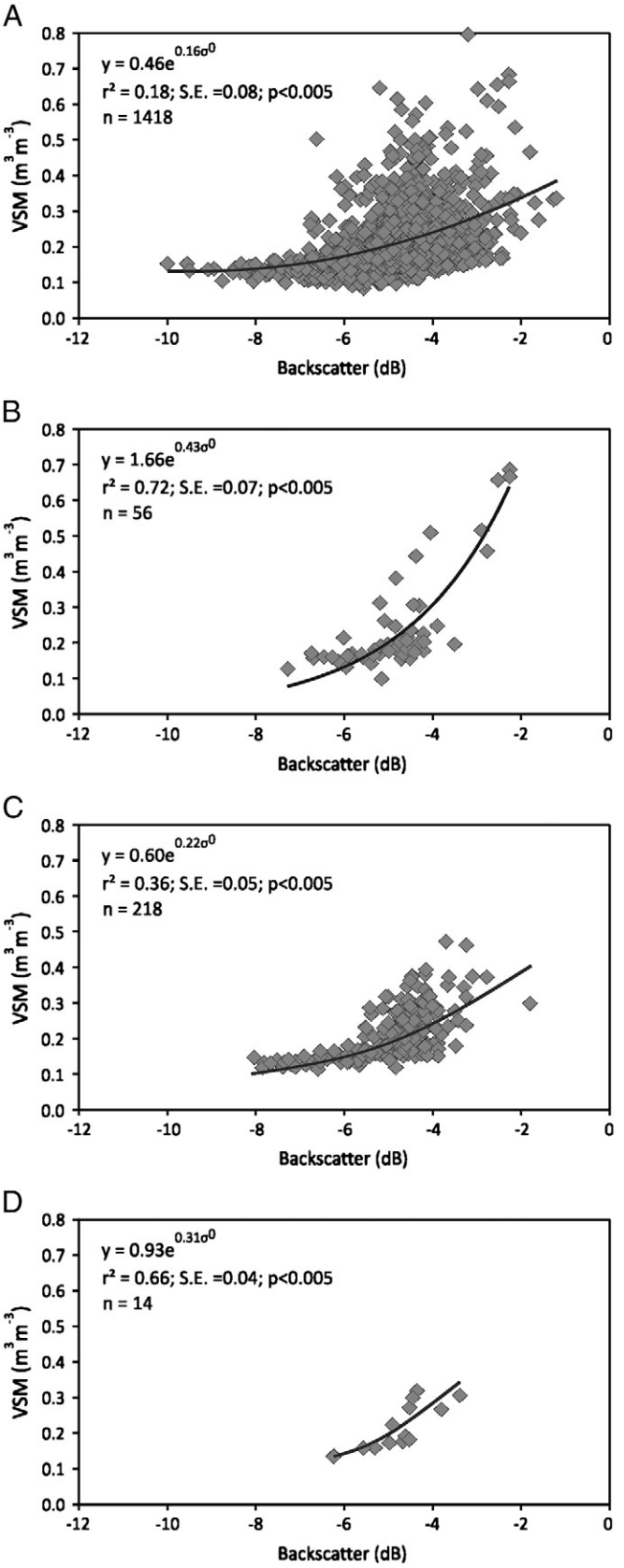

Fig. 7. Exponential growth relationships between VSM and backscatter coefficient averaged at (A) 25 m pixel spatial averaging scale; (B) topographic feature scale; (C) basin scale; and (D) parcel scale.

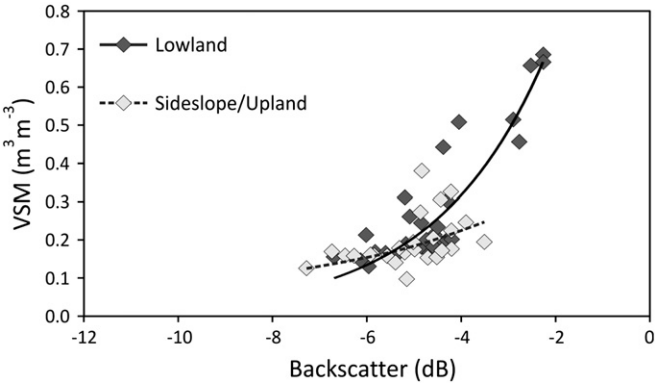

Fig. 8. Exponential growth relationships between VSM and backscatter coefficient averaged at the topographic feature scale per lowland ($1.75e^{0.43\sigma^0}$; n = 31; $R^2 = 0.81$; S.E. = 0.09; $P<0.005$) and sideslope and upland ($0.46e^{0.17\sigma^0}$; n = 25; $R^2 = 0.20$; S.E. = 0.06; $P<0.005$) feature types.

averaging schemes. We then compared the performance of empirical models relating spatially averaged backscatter coefficient and VSM developed from the different spatial averaging schemes.

A decrease in heterogeneity in backscatter coefficient was found with increasing coarseness of spatial averaging from image pixels to drainage basins to parcels. The decreasing heterogeneity corresponded with improvements in the strength of exponential models relating backscatter coefficient and VSM developed at the pixel ($R^2 = 0.18$), basin ($R^2 = 0.36$) and parcel ($R^2 = 0.66$) scales. Similar findings were reported by Álvarez-Mozos et al. (2005) in the low relief La Tejería watershed of northern Spain, where weak linear relationships at the pixel scale ($R^2 = 0.30$–0.37) were improved when averaged at agricultural field ($R^2 = 0.44$–0.82) and drainage basin scales ($R^2 = 0.86$). Similarly, other studies including Cognard et al. (1995), Koyama et al. (2010), Moran et al. (2000), and Thoma et al. (2004) found improvements in relationships developed at increasing spatial averaging scales in a variety of low relief landscapes.

Improvements in the strength of the relationships at coarser spatial averaging scales were attributed to the decrease in heterogeneity of backscatter response to random noise as well as surface effects that include VSM. In fact, these improvements were associated with decreases in the heterogeneity of VSM that were greater than those of the backscatter response. This indicated a loss of information content related to VSM.

We found that spatial averaging at the scale of topographic features preserved a larger range of VSM values present in backscatter pixels than in coarser scales. In contrast to spatial averaging at coarser scales, the reduction in the range of VSM values at the scale of topographic features was smaller than in the range of backscatter coefficients. A greater portion of the backscatter response to VSM was preserved at this scale in relation to random noise or response to unknown surface effects. This finding was consistent with our expectations that topography is an important spatial control on the distribution of VSM that affects backscatter response in prairie pothole basins.

Table 5
Comparison of linear and exponential growth models relating volumetric soil moisture (VSM) content to backscatter coefficient averaged at the topographic feature scale per lowland and combined sideslope and upland feature types.

	n	Equation	R^2	S.E.	Normality	Constant variance	P
Linear							
Lowland	31	$0.86 + 0.13\sigma^0$	0.71	0.09	Failed	Passed	<0.005
Sideslope/upland	25	$0.36 + 0.03\sigma^0$	0.21	0.06	Failed	Failed	<0.005
Exponential							
Lowland	31	$1.75e^{0.43\sigma^0}$	0.81	0.07	Passed	Passed	<0.005
Sideslope/upland	25	$0.46e^{0.17\sigma^0}$	0.20	0.06	Passed	Passed	<0.005

Table 6
Exponential growth models relating volumetric soil moisture (VSM) content (θ) to backscatter coefficient averaged at the pixel, topographic feature, basin and parcel scales using 104 randomly selected backscatter image pixels to examine whether the success of the model at the topographic feature scale could be attributed to sampling fewer backscatter image pixels.

	n	Equation	R^2	S.E.	Normality	Constant variance	P
Pixel	104	$0.37e^{0.12\sigma^0}$	0.17	0.06	Failed	Failed	<0.005
Topographic feature	96	$0.98e^{0.26\sigma^0}$	0.25	0.17	Failed	Failed	<0.005
Basin	79	$0.36e^{0.17\sigma^0}$	0.18	0.06	Failed	Failed	<0.005
Parcel	14	$0.51e^{0.18\sigma^0}$	0.36	0.05	Passed	Passed	0.03

The strongest relationship between backscatter coefficient and VSM was found in the exponential model developed at the topographic feature spatial averaging scale ($R^2 = 0.72$, $P<0.005$). This improvement in model performance was related to topographic controls on VSM, as demonstrated by increases in both mean VSM and backscatter coefficient with decreases in elevation from upland to sideslope to lowland features. This improvement may also be related to topographically controlled surface characteristics that influence backscatter coefficient that were not considered explicitly in this study (e.g., surface geometry or roughness). However, relationships between backscatter coefficient and VSM developed at the pixel and at coarser spatial averaging scales showed strong improvements using only pixel samples of uniform topographic features. These findings demonstrate that mixed topographic features produce a substantial portion of backscatter noise (i.e., pixels containing heterogeneous terrain). This illustrates the importance of isolating the tendency of backscatter response in topographic features and the suitability of using topographic features as a basis for spatial averaging of backscatter coefficient.

The improved performance of the exponential over the linear model may be explained by the integration of a slightly positive linear trend for the drier topographic features with a strongly positive linear trend for the wetter topographic features. The dominant contribution of wetter lowland features to the overall strength of the model suggests that these features define areas of uniform VSM with minimal interference from other surface effects. In contrast, the less dominant contribution of the other topographic features suggests areas of less uniform VSM and/or greater interference of surface effects that may occur on the drier sideslope and upland features. Calibration for other surface parameters in these higher topographic features may improve the performance of the model.

The exponential model developed from spatial averaging at the scale of topographic features captures the physical process of water movement down hillslopes, as represented in a greater range of VSM. Compared to other landscape-based spatial averaging schemes (i.e., drainage basins or arbitrary parcels), the finer scale of topographic features provides a more detailed spatial estimation of VSM across the natural prairie pothole landscape. The exponential model was developed on a natural prairie pothole landscape. While its

Table 7
Exponential growth models relating volumetric soil moisture (VSM) content to backscatter coefficient averaged at the pixel, basin and parcel scales using the 104 backscatter image pixel samples used to develop the topographic feature averaging scheme to examine the effects of including only unmixed pixels.

	n	Equation	R^2	S.E.	Normality	Constant variance	P
Pixel	104	$1.55e^{0.43\sigma^0}$	0.58	0.07	Failed	Failed	<0.005
Basin	48	$1.75e^{0.44\sigma^0}$	0.74	0.07	Passed	Failed	<0.005
Parcel	14	$1.80e^{0.45\sigma^0}$	0.80	0.04	Passed	Passed	<0.005

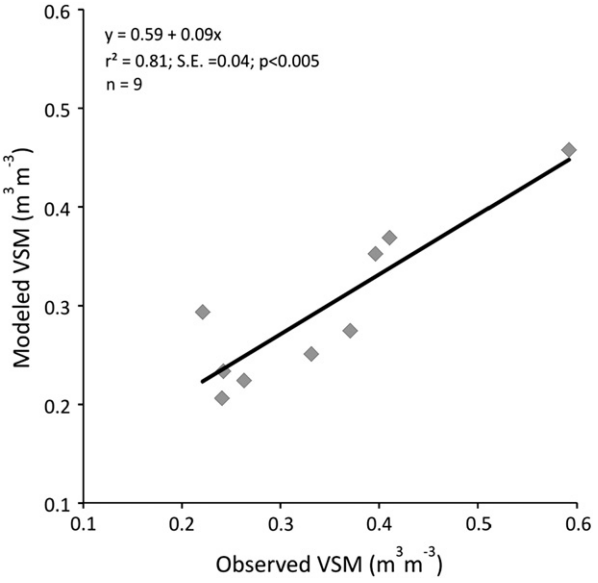

Fig. 9. Linear relationship between observed and modeled VSM at the topographic feature scale for test image at P3 (September 7).

application to "working" landscapes with different agricultural covers would require further testing, our topographic approach to spatial averaging of backscatter coefficient holds promise for scientific and management applications that require finer scale estimations of VSM. Furthermore, with the recent launch of sensors such as RADARSAT-2, with spatial resolution of about 5 m, the potential of using topographic features to defining even finer scale estimates of VSM may be realized.

5. Conclusions

The combined use of topographic features derived from fine resolution digital elevation models and SAR data offers improvement in models for estimating volumetric soil moisture (VSM) on complex landscapes. Compared with coarser spatial averaging schemes, spatial averaging of SAR backscatter coefficient and VSM based on topographic features (uplands, sideslopes and lowlands) (1) captured more of the natural heterogeneity of VSM found in natural prairie pothole landscapes; (2) reduced the heterogeneity of backscatter response unrelated to VSM signals; (3) improved the performance of an empirical model relating backscatter coefficient and VSM, and (4) provided a more detailed spatial estimation of VSM within prairie pothole basins. These findings imply that the physical processes

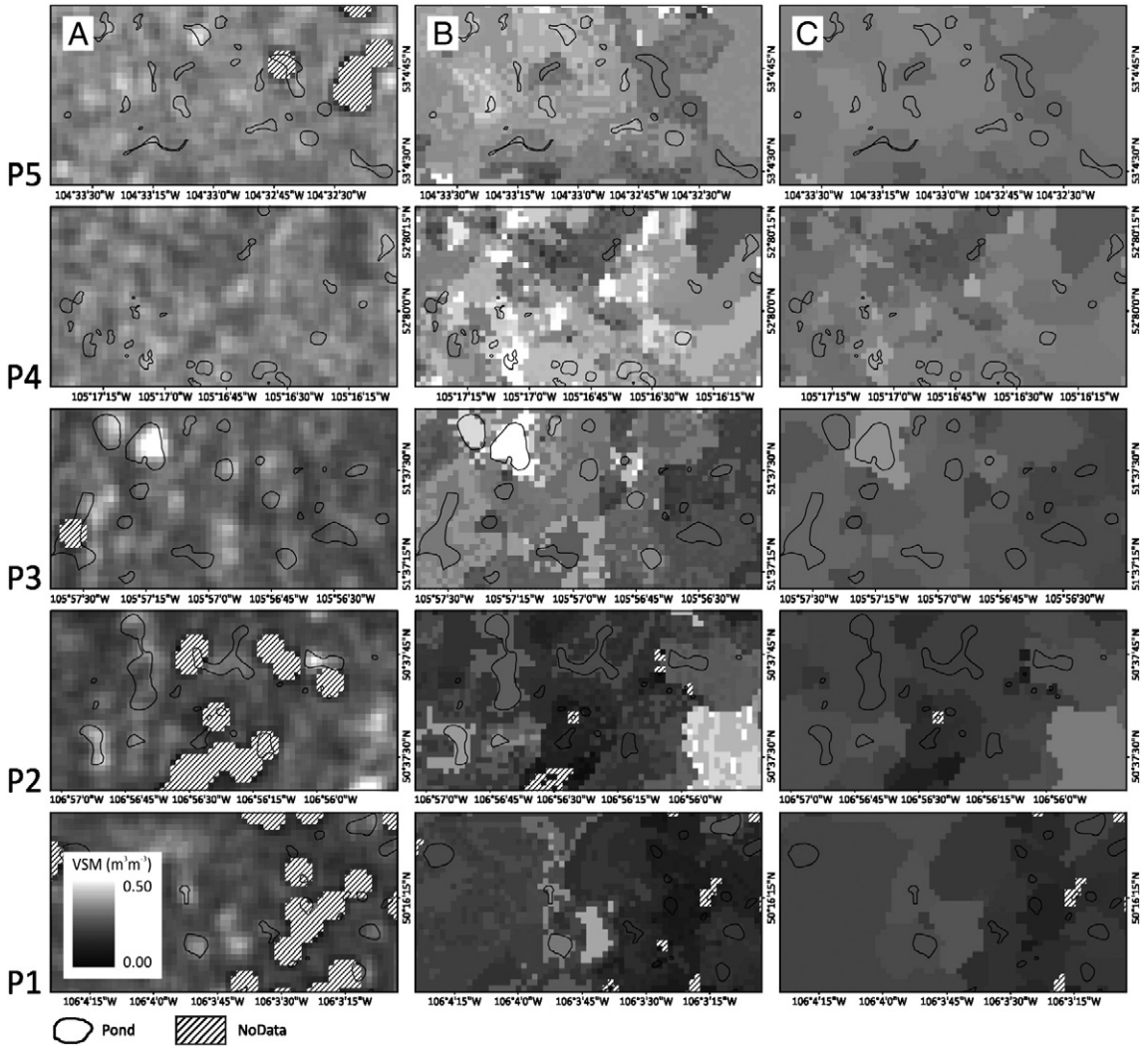

Fig. 10. Areal soil moisture maps of P1 (August 7), P2 (August 7), P3 (August 14), P4 (July 28) and P5 (July 28) from exponential models developed at (A) pixel scale; (B) topographic feature scale; and (C) basin scale.

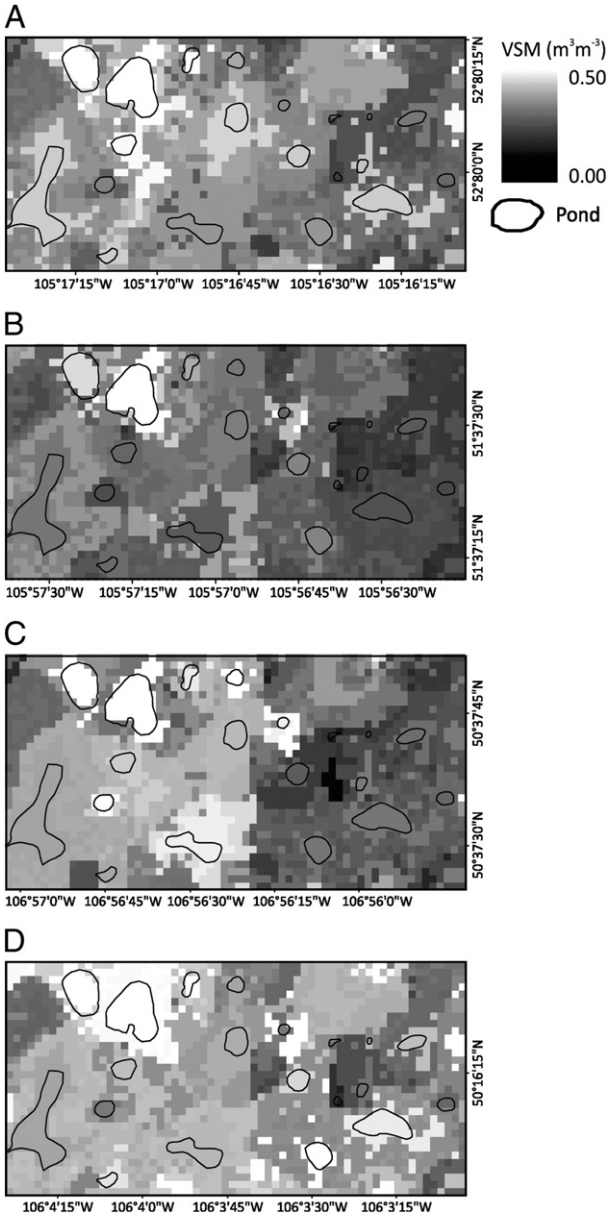

Fig. 11. Areal soil moisture maps of P3 using topographic feature model: (A) July 21; (B) August 14; (C) September 7; and (D) October 1.

influencing VSM distribution should be considered when developing spatial averaging schemes for mapping soil moisture from backscatter coefficients.

Acknowledgments

We gratefully acknowledge the anonymous reviewers, whose careful critique of the original manuscript significantly improved the manuscript. This research was funded by a Natural Sciences and Engineering Research Council of Canada (NSERC) Discovery Grant, a Network of Centres of Excellence — Sustainable Forest Management Grant ("Physically based tools for generating maps of hydrologically sensitive areas for use in forest operations planning"), and a Ducks Unlimited Canada Grant ("Hydrologic profiling for greenhouse gasses on the Prairie Potholes") to IFC. We acknowledge Dr. R. McDougal for funding this research; Dr. R. Bourbonnière, National Water Research Institute, Environment Canada for providing access to the RADARSAT-1 data; and Tarrah Fairweather and Sarah Harper for the long hours and hard work they completed during the summer field campaign.

References

Álvarez-Mozos, J., Casalí, J., González-Audícana, M., & Verhoest, N. E. C. (2005). Correlation between ground measured soil moisture and RADARSAT-1 derived backscattering coefficient over an agricultural catchment of Navarre (North of Spain). *Biosystems Engineering*, *92*, 119–133.

Beven, K., & Kirkby, M. J. (1979). A physically based, variable contributing area model of basin hydrology. *Hydrological Sciences – Bulletin – des Sciences Hydrologiques*, *24*, 43–69.

Carlyle, S. (2006). The changing nature of topographic controls on soil moisture in prairie pothole complexes along a climatic gradient. Unpublished MSc Thesis. Department of Geography, The University of Western Ontario, London, Ontario.

Cognard, A. L., Loumagne, C., Normand, M., Olivier, P., Ottlé, C., Vidal-Madjar, D., et al. (1995). Evaluation of the ERS 1/synthetic aperture radar capacity to estimate surface soil moisture: Two-year results over the Naizin watershed. *Water Resources Research*, *31*, 975–982.

Delta-T Devices (1999). Cambridge, England: ThetaProbe ML2x.

Famiglietti, J. S., Rudnicki, J. W., & Rodell, M. (1998). Variability in surface moisture content along a hillslope transect: Rattlesnake Hills, Texas. *Journal of Hydrology*, *210*, 259–281.

Fung, K. I. (1969). Natural vegetation. In J. H. Richards (Ed.), *Atlas of Saskatchewan* (pp. 263). Saskatoon, Saskatchewan: Modern Press.

Government of Canada, Natural Resources Canada, Earth Sciences Sector, Centre for Topographic Information. (2000). Canadian Digital Elevation Data. http://www.geobase.ca/geobase/en/find.do?produit=cded.

Government of Canada, Natural Resources Canada, Earth Sciences Sector, Centre for Topographic Information. (2007). Canada: National Hydro Network. http://www.geobase.ca/geobase/en/data/nhn/index.html.

Government of Canada, Natural Resources Canada, Earth Sciences Sector, Centre for Topographic Information. (2007). Canada: National Road Network. http://www.geobase.ca/geobase/en/data/nrn/index.html.

Hamon, W. R. (1963). Computation of direct runoff amounts from storm rainfall. *International Association Hydrological Science*, *63*, 52–62.

Koyama, C. N., Korres, W., Fiener, P., & Schneider, K. (2010). Variability of surface soil moisture observed from multitemporal C-Band Synthetic Aperture Radar and field data. *Vadose Zone Journal*, *9*, 1014–1024.

Lievens, H., Verhoest, N. E. C., De Keyser, E., Vernieuwe, H., Matgen, P., Álvarez-Mozos, J., et al. (2010). Effective roughness modelling as a tool for soil moisture retrieval from C-and L-band SAR. *Hydrology and Earth System Sciences*, *15*, 151–162.

Lievens, H., Vernieuwe, H., Álvarez-Mozos, J., De Baets, B., & Verhoest, N. E. C. (2009). Error in radar-derived soil moisture due to roughness parameterization: An analysis based on synthetical surface profiles. *Sensors*, *9*, 1067–1093.

Lopes, A., Nezry, E., Touzi, R., & Laur, H. (1993). Structure detection and statistical adaptive speckle filtering in SAR images. *International Journal of Remote Sensing*, *14*, 1735–1758.

MacMillan, R. A. (2000). *A protocol for Preparing Digital Elevation (DEM) data for input and analysis using the Landform Segmentation Model (LSM) Programs: Second draft 02/2000.* Edmonton, Alberta: LandMapper Environmental Solutions.

Moran, M. S., Hymer, D. C., Qi, J., & Sano, E. S. (2000). Soil moisture evaluation using multi-temporal synthetic aperture (SAR) in semiarid rangeland. *Agricultural and Forest Meteorology*, *105*, 69–80.

Oldak, A., Jackson, T. J., Starks, P., & Elliott, R. (2003). Mapping near-surface soil moisture on regional scale using ERS-2 SAR data. *International Journal of Remote Sensing*, *24*, 4579–4598.

PCI Geomatics (2007). (Version 10.1) [computer software]. Ontario: Richmond Hill.

Quesney, A., Le Hégarat -Mascle, S., Taconet, O., Vidal-Madjar, D., Wigneron, J. P., Loumagne, C., et al. (2000). Estimation of watershed soil moisture index from ERS/SAR data. *Remote Sensing of Environment*, *72*, 290–303.

Scott, G. A. (1995). *Canada's vegetation: A world perspective.* Montreal, Quebec: McGill-Queen's University Press.

Shepherd, N. W. (2000). Extraction of beta nought and sigma nought from RADARSAT CDPF products. *CSA Document AS97-5001 Rev. 4*. Ottawa, Ontario: ALTRIX Systems.

Stewart, R. E., & Kantrud, H. A. (1971). Classification of natural ponds and lakes in the glaciated prairie region. *Resource Publication 92*. Washington, DC: Bureau of Sport Fisheries and Wildlife, U.S. Fish and Wildlife Service.

Systat Software (2008). *SigmaPlot (Version 11.0) [computer software]. San Jose, California.*

Thoma, D. P., Moran, M. S., Bryant, R., Collins, C. H., Rahman, M., & Skirvin, S. (2004). Comparison of two methods for extracting surface soil moisture from C-band radar imagery. *IEEE Transactions on Geoscience and Remote Sensing*, *2*, 827–830.

Thoma, D. P., Moran, M. S., Bryant, R., Rahman, M. M., Holifield Collins, C. D., Keefer, T. O., et al. (2008). Appropriate scale of soil moisture retrieval from high resolution radar imagery for bare and minimally vegetated soils. *Remote Sensing of Environment*, *112*, 403–414.

Verhoest, N. E. C., Lievens, H., Wagner, W., Álvarez-Mozos, J., Moran, M. S., & Mattia, F. (2008). On the soil roughness parameterization problem in soil moisture retrieval of bare surfaces from synthetic aperture radar. *Sensors*, *8*, 4213–4248.

Webster, K. L., Creed, I. F., Beall, F. D., & Bourbonnière, R. A. (2011). A topographic template for estimating soil carbon pools in forested catchments. *Geoderma*, *160*, 457–467.

Western, A. W., & Blöschl, G. (1999). On the spatial scaling of soil moisture. *Journal of Hydrology*, *217*, 203–224.

Western, A. W., Grayson, R. B., Blöschl, G., Willgoose, G. R., & McMahon, T. A. (1999). Observed spatial organization of soil moisture and its relation to terrain indices. *Water Resources Research*, *35*, 797–810.